Soret, M., et al., 2021, How Himalayan collision stems from subduction: Geology, v. 49, https://doi.org/10.1130/G48803.1

SUPPLEMENTAl MATERIAL

1) Electron microscopy

Electron probe microanalysis was carried out in the Fipke Laboratory for Trace Element Research (FiLTER) at University of British Columbia Okanagan (Kelowna, Canada) using a Cameca SX-Five-FE instrument to quantify major element compositions. Point measurements and composition maps were made using classical analytical conditions: 15 kV acceleration voltage and 10 nA beam current allowing ~1 μm beam size in wavelength-dispersive spectroscopy mode for the point analyses, and 15 kV, 40 nA with a 4 μm spatial resolution for the maps. The instrument was calibrated against mineral and oxide reference material from CF Minerals and Micro Analysis Consultants. Data are reported in Table S1 and in Figure S1 (Supp. Mat).

2) U–Pb petrochronology

In situ LASS U–Pb petrochronology was performed on titanite at the University of California, Santa Barbara (USA) following methods outlined in Kylander-Clark et al. (2013) with modifications presented in McKinney et al., 2015. U–Pb isotope data were measured using a Nu Instruments Multicollector-Inductively Coupled Plasma Mass Spectrometer (MC-ICP-MS) while trace element concentrations were collected on an Agilent 7700S quadrupole ICP-MS. Both mass spectrometers were coupled to a Cetac / Teledyne Photon Machines excimer laser (193 nm wavelength) ablation system operated at 4 Hz repetition rate, 6 J/cm^2 laser fluence, and 25 μm diameter laser spot size. Analyses consisted of 20s of data followed by 15s washout. The following elements were measured: Pb, U, Th, Al, Si, Ca, Ti, V, Fe, Rb, Sr, Y, Zr, Nb, La, Ce, Pr, Nd, Sm, Eu, Gd, Tb, Dy, Ho, Er, Tm, Yb, Lu, Hf, Ta.

Titanite unknowns were bracketed by analyses of primary and secondary standards. MKED was used as a primary reference titanite (ID-TIMS ages of $^{206}Pb/^{207}Pb$: 1521.02 ± 0.55 Ma; $^{207}Pb/^{235}U$: 1518.87 ± 0.31Ma; $^{206}Pb/^{238}U$: 1517.32 ± 0.32 Ma; Spandler et al., 2016). BLR (Bear Lake Road; 1047 ± 1 Ma (ID-TIMS); Aleinikoff et al., 2006) and Y1710C5 (388.6 ± 0.5 Ma (ID-TIMS), Spencer et al., 2013) were used as a secondary RMs and returned weighted-mean $^{206}Pb/^{238}U$ ages of 1063 ± 2 Ma (2σ, mean squares weighted distribution (MSWD) of 0.64, N = 56). and 385 ± 1 Ma (2σ, MSWD = 0.69) respectively. Trace element data were normalized to BHVO (Wilson, 1997) assuming stoichiometric Ti. A ^{207}Pb-based

common Pb correction was applied to titanite $^{238}U/^{206}Pb$ dates as implemented in IsoplotR (Vermeesch, 2018). Data are reported in Tables S2 (ages) and S3 (trace elements) (Supp. Mat).

3) Pressure–Temperature estimates

Multi-equilibrium thermobarometry was carried out using the THERMOCALC program in the Average P-T mode (Powell and Holland, 1994) for both specimens. Mineral activities were calculated with the AX software (https://www.esc.cam.ac.uk/research/research-groups/research- projects/tim-hollands-software-pages/ax). The assemblage garnet rim + biotite + plagioclase + muscovite + quartz + water yields peak P–T estimates of 660 ± 30°C and 1.0 ± 0.1 GPa for specimen H65 and 670 ± 30°C and 1.1 ± 0.1 GPa for specimen H37 (Fig. 2B).

These results are consistent with the Zr-in-titanite isopleths (calibration of Hayden et al., 2008; Fig. 2B) calculated from inclusions in garnet outer rims. The Ti-in-biotite thermometer applied to Ti-rich biotite from the matrix (Henry et al., 2005) also indicates similar peak-T conditions (650 ± 25°C; Fig. S1B). Ti-in-quartz (7-10 ppm (12 analyses); calibration of Thomas et al., 2010; Fig. S1D) and Zr-in-titanite (5-10 ppm) isopleths for inclusions in garnet inner rims yield lower temperatures at similar pressure condition (~595°C – 1.0 GPa), consistent with the Ti-in-biotite thermometry derived from a biotite inclusion in the same relative position (590 ± 25°C; i.e. grey box in Fig. 2A). It should be noted that quartz found in the outer rim yielded values below the detection limit. Since these grains are also in contact with the matrix (see Fig. 2A), they might have been affected by a late recrystallization during the retrograde history or a change in Ti activity.

P-T conditions for the prograde titanite dates with an intermediate Zr content (Figs. 2C, D) were estimated at 1 GPa according to the prograde path independently constrained (Fig. 2B). Pink and blue arrows outline the prograde and retrograde evolution, respectively.

4) Compilation of (U)HP rocks in worldwide orogenic systems (Figure 3)

The following references were used to draw the P–T–t paths in Figures 3 and S3: 1: (St-Onge et al., 2013); 2: (de Sigoyer et al., 2000); 3: (Guillot et al., 2008); 4: (Wilke et al., 2010); 5: (Kaneko et al., 2003); 6: (Donaldson et al., 2013); 7: (Weller and St-Onge, 2017), 8: (Lardeaux, 2014); 9: (Schmid et al., 2013).

References

Aleinikoff, J.N., Schenck, W.S., Plank, M.O., Srogi, L.A., Fanning, C.M., Kamo, S.L., and Bosbyshell, H., 2006, Deciphering igneous and metamorphic events in high-grade rocks of the Wilmington complex, Delaware: Morphology, cathodoluminescence and backscattered electron zoning, and SHRIMP U-Pb geochronology of zircon and monazite: Bulletin of the Geological Society of America, v. 118, p. 39–64, doi:10.1130/B25659.1.

Donaldson, D.G., Webb, A.A.G., Menold, C.A., Kylander-Clark, A.R.C., and Hacker, B.R., 2013, Petrochronology of himalayan ultrahigh-pressure eclogite: Geology, v. 41, p. 835–838, doi:10.1130/G33699.1.

Guillot, S., Mahéo, G., de Sigoyer, J., Hattori, K.H., and Pêcher, A., 2008, Tethyan and Indian subduction viewed from the Himalayan high- to ultrahigh-pressure metamorphic rocks: Tectonophysics, v. 451, p. 225–241, doi:10.1016/j.tecto.2007.11.059.

Hayden, L.A., Watson, E.B., and Wark, D.A., 2008, A thermobarometer for sphene (titanite): Contributions to Mineralogy and Petrology, v. 155, p. 529–540, doi:10.1007/s00410-007-0256-y.

Henry, D.J., Guidotti, C. V., and Thomson, J.A., 2005, The Ti-saturation surface for low-to-medium pressure metapelitic biotites: Implications for geothermometry and Ti-substitution mechanisms: American Mineralogist, v. 90, p. 316–328, doi:10.2138/am.2005.1498.

Kaneko, Y., Katayama, I., Yamamoto, H., Misawa, K., Ishikawa, M., Rehman, H.U., Kausar, A.B., and Shiraishi, K., 2003, Timing of Himalayan ultrahigh-pressure metamorphism: Sinking rate and subduction angle of the Indian continental crust beneath Asia: Journal of Metamorphic Geology, v. 21, p. 589–599, doi:10.1046/j.1525-1314.2003.00466.x.

Kylander-Clark, A.R.C., Hacker, B.R., and Cottle, J.M., 2013, Laser-ablation split-stream ICP petrochronology: Chemical Geology, v. 345, p. 99–112, doi:10.1016/j.chemgeo.2013.02.019.

Lardeaux, J.M., 2014, Deciphering orogeny: A metamorphic perspective examples from european alpine and variscan belts Part II: Variscan metamorphism in the french massif central - A review: Bulletin de la Societe Geologique de France, v. 185, p. 281–310, doi:10.2113/gssgfbull.185.2.93.

Powell, R., and Holland, T., 1994, Optimal geothermometry and geobarometry: American Mineralogist, v. 79, p. 120–133.

Schmid, S.M., Scharf, A., Handy, M.R., and Rosenberg, C.L., 2013, The Tauern Window (Eastern Alps, Austria): A new tectonic map, with cross-sections and a

tectonometamorphic synthesis: Swiss Journal of Geosciences, v. 106, p. 1–32, doi:10.1007/s00015-013-0123-y.

de Sigoyer, J. De, Géologie, I. De, Argand, E., Centre, J.B., De, N., Scientifique, R., Cedex, L., and Luais, B., 2000, Dating the Indian continental subduction and collisional thickening in the northwest Himalaya : Multichronology of the Tso Morari eclogites: Geology, v. 28, p. 487–490.

Spandler, C., Hammerli, J., Sha, P., Hilbert-wolf, H., Hu, Y., Roberts, E., and Schmitz, M., 2016, MKED1 : A new titanite standard for in situ analysis of Sm–Nd isotopes and U–Pb geochronology: Chemical Geology, v. 425, p. 110–126, doi:10.1016/j.chemgeo.2016.01.002.

Spencer, K.J., Hacker, B.R., Kylander-clark, A.R.C., Andersen, T.B., Cottle, J.M., Stearns, M.A., Poletti, J.E., and Seward, G.G.E., 2013, Campaign-style titanite U–Pb dating by laser-ablation ICP : Implications for crustal flow, phase transformations and titanite closure: Chemical Geology, v. 341, p. 84–101, doi:10.1016/j.chemgeo.2012.11.012.

St-Onge, M.R., Rayner, N., Palin, R.M., Searle, M.P., and Waters, D.J., 2013, Integrated pressure-temperature-time constraints for the Tso Morari dome (Northwest India): Implications for the burial and exhumation path of UHP units in the western Himalaya: Journal of Metamorphic Geology, v. 31, p. 469–504, doi:10.1111/jmg.12030.

Thomas, J.B., Watson, E.B., Spear, F.S., Shemella, P.T., Nayak, S.K., and Lanzirotti, A., 2010, TitaniQ under pressure: The effect of pressure and temperature on the solubility of Ti in quartz: Contributions to Mineralogy and Petrology, v. 160, p. 743–759, doi:10.1007/s00410-010-0505-3.

Vermeesch, P., 2018, Geoscience Frontiers IsoplotR : A free and open toolbox for geochronology: Geoscience Frontiers, v. 9, p. 1479–1493, doi:10.1016/j.gsf.2018.04.001.

Weller, O.M., and St-Onge, M.R., 2017, Record of modern-style plate tectonics in the Palaeoproterozoic Trans-Hudson orogen: Nature Geoscience, v. 10, p. 305–311, doi:10.1038/ngeo2904.

Wilke, F.D.H., O'Brien, P.J., Gerdes, A., Timmerman, M.J., Sudo, M., and Khan, M.A., 2010, The multistage exhumation history of the Kaghan Valley UHP series, NW Himalaya, Pakistan from U-Pb and 40Ar-39Ar ages: European Journal of Mineralogy, v. 22, p. 703–719, doi:10.1127/0935-1221/2010/0022-2051.

Wilson, S.A., 1997, Data compilation for USGS reference material BHVO-2, Hawaiian basalt. US geological survey open-file report.:

SUPPLEMENTAL MATERIAL CAPTIONS

Figure S1. A: Representative compositional profiles in zoned garnet crystal from specimen H65. B: Titanium vs. Mg# in biotite from specimens H65 and H37. Isotherms were calculated using the Ti-in-biotite thermometer of Henry et al. (2005). C: (Gd/Yb) ratios (ppm) vs. 207Pb-corrected 238U/206Pb ages in titanite from specimens H65 and H37.

Figure S2. Representative mineral assemblages in the studied specimens H65 and H37.

Figure S3. Larger example of Figure 3 with all the references included directly in the figure.

Table S1. Selected representative analyses of garnet, micas and feldspar from point analysis.

Table S2. U-Pb Titanite dates from the analyzed specimens of the Swat region.

Table S3. Trace elements composition of titanite from the analyzed specimens of the Swat region.

Table S4. Parageneses of analysed specimens and corresponding GPS coordinates from the Swat region.

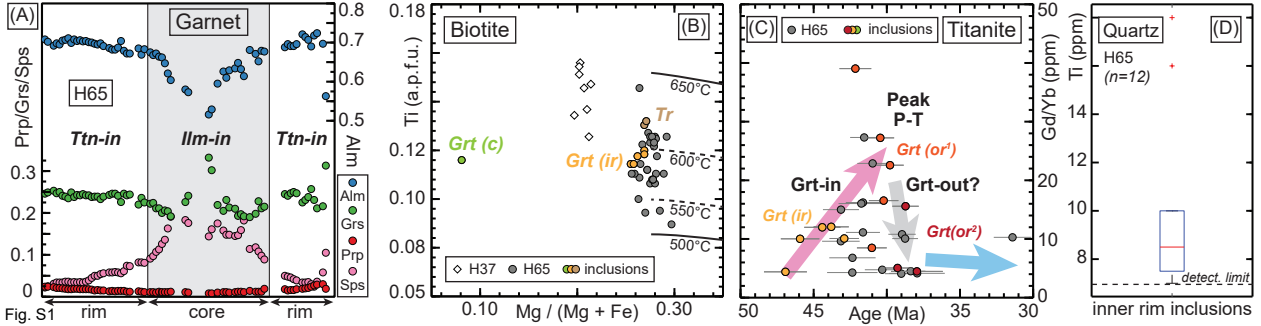
(A)
Garnet
H65
Ttn-in
Ilm-in
Ttn-in
Prp/Grs/Sps
Alm
Alm
Grs
Prp
Sps
rim
core
rim
(B)
Biotite
Ti (a.p.f.u.)
Mg / (Mg + Fe)
Grt (c)
Grt (ir)
Tr
650°C
600°C
550°C
500°C
H37
H65
inclusions
(C)
H65
inclusions
Titanite
Peak
P-T
Grt-in
Grt-out?
Grt (ir)
Grt (or¹)
Grt(or²)
Gd/Yb (ppm)
Age (Ma)
(D)
Quartz
H65
(n=12)
Ti (ppm)
detect. limit
inner rim inclusions

Fig. S1

Fig. S2

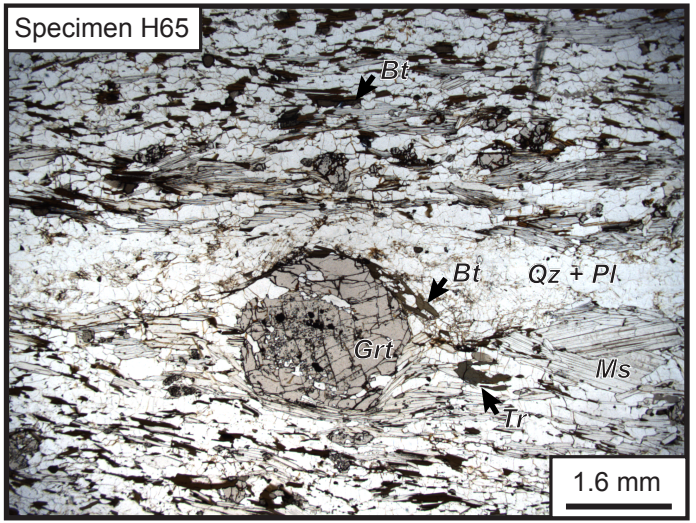
Specimen H65
Bt
Bt
Qz + Pl
Grt
Ms
Tr
1.6 mm

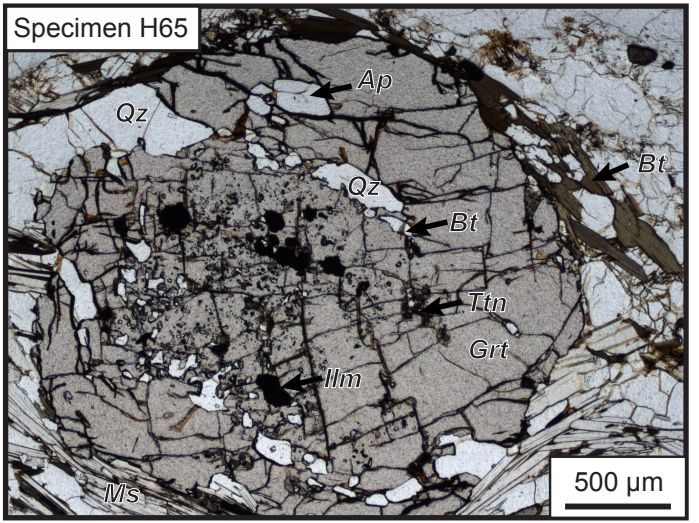
Specimen H65
Ap
Qz
Qz
Bt
Bt
Ttn
Grt
Ilm
Ms
500 µm

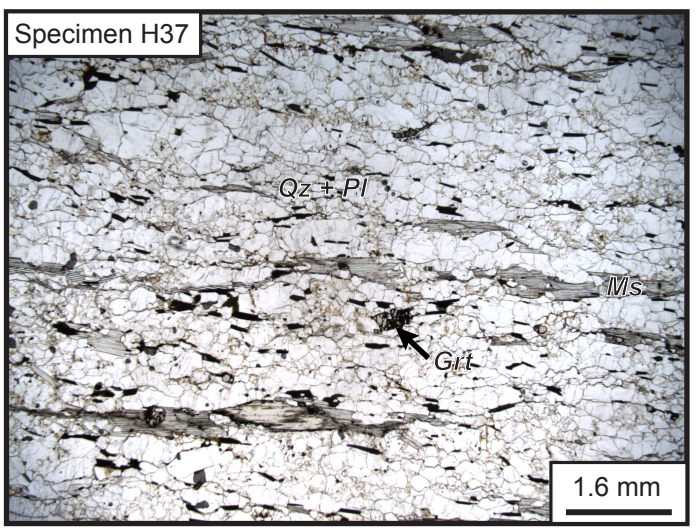
Specimen H37
Qz + Pl
Ms
Grt
1.6 mm

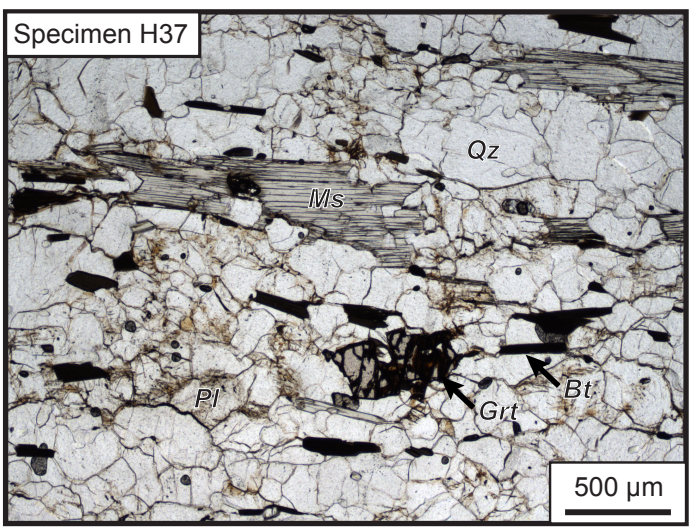
Specimen H37
Qz
Ms
Pl
Grt
Bt
500 µm

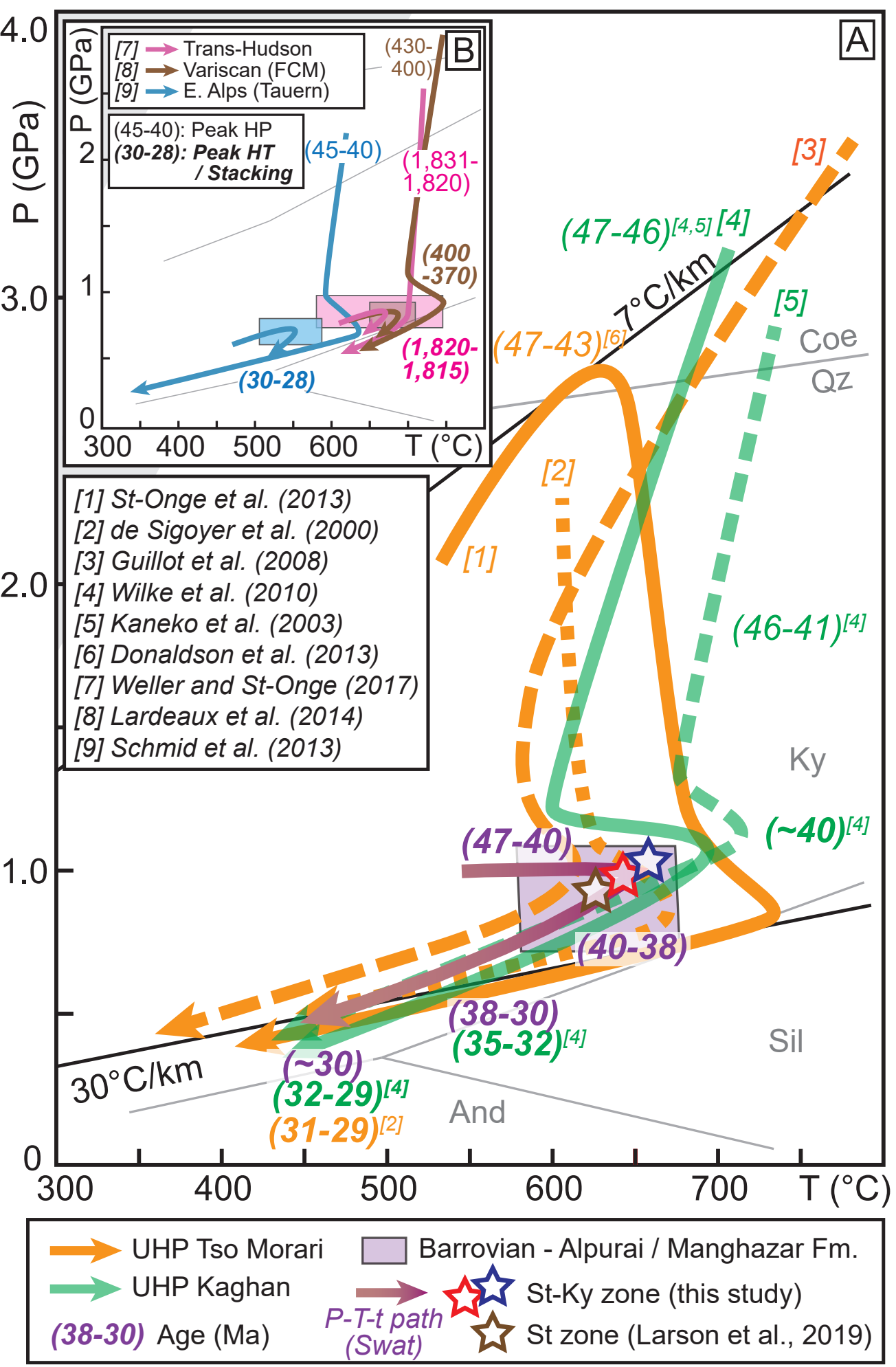
A
B
P (GPa)
T (°C)
[7] Trans-Hudson
[8] Variscan (FCM)
[9] E. Alps (Tauern)
(45-40): Peak HP
(30-28): Peak HT / Stacking
(430-400)
(1,831-1,820)
(400-370)
(1,820-1,815)
(45-40)
(30-28)
[1] St-Onge et al. (2013)
[2] de Sigoyer et al. (2000)
[3] Guillot et al. (2008)
[4] Wilke et al. (2010)
[5] Kaneko et al. (2003)
[6] Donaldson et al. (2013)
[7] Weller and St-Onge (2017)
[8] Lardeaux et al. (2014)
[9] Schmid et al. (2013)
(47-46)[4,5] [4]
[3]
[5]
7°C/km
(47-43)[6]
[1]
[2]
Coe
Qz
(46-41)[4]
Ky
(~40)[4]
(47-40)
(40-38)
(38-30)
(35-32)[4]
Sil
30°C/km
(~30)
(32-29)[4]
(31-29)[2]
And
UHP Tso Morari
UHP Kaghan
(38-30) Age (Ma)
Barrovian - Alpurai / Manghazar Fm.
P-T-t path (Swat)
St-Ky zone (this study)
St zone (Larson et al., 2019)